Metal Phthalocyanine–Fullerene Dyads: Promising Lamellar Columnar Donor–Acceptor Liquid Crystal Phases

Matthias Lehmann,*[a, b] Moritz Dechant,[a] Dominik Weh,[a] and Emely Freytag[a]

Liquid crystal (LC) shape-amphiphiles with a disc tethered to a fullerene have been intensely studied for the application in photovoltaics, and helical nanosegregation of C_{60} has been claimed around the π-stacking disks based on X-ray results. The most promising materials reported to date have been resynthesized and studied comprehensively by XRS, density measurements, modelling, and electron density reconstruction. In contrast to previous reports, the results indicate that metal phthalocyanine–fullerene mesogens pack in lamellar columnar phases with p2gm symmetry. Fullerenes assemble in layers and are flanked by phthalocyanine columns, thus explaining the balanced charge carrier mobility of electrons and holes. Such variable donor–acceptor structures are promising for organic electronic applications.

Discotic mesogens have been intensely studied in the last two to three decades as hole conducting materials owing to their promising charge carrier mobilities.[1] It was thus an obvious idea to tether such mesogens to an electron acceptor forming double cables.[2] Since discotic liquid crystals can frequently be homeotropically aligned between two substrates,[3] which is obligatory in a photovoltaic (PV) device, such double cable materials were proposed to be auspicious for organic PV cells. Phthalocyanines and porphyrins, which show absorption of the visible light over a broad portion of the solar spectrum and are well known discotic mesogens with high charge carrier mobilities, have been subsequently attached to the broadly used, excellent electron acceptor, fullerene C60.[2,4] Many of these systems have been claimed to be columnar liquid crystals with helically arranged fullerenes in the periphery.[2c,i,j,4a] High ambipolar and balanced hole and electron mobilities,[2c] long-lived charge separated states,[5] and facile homeotropic alignment have been reported.[2i,j] Indeed, these properties would be perfect for the production of photovoltaic cells, however, to the best of our knowledge no PV cell with aligned LC phthalocyanine-fullerene dyads has been reported today. We became recently interested in these materials, since star-shaped, shape-persistent mesogens with benzene and phthalocyanine cores (e.g. compounds **3a**,**b** in Figure 1) and fullerenes as guests hidden between the arm scaffold of the stars truely self-assemble in helical stacks but are difficult to align homeotropically.[6][7] Since the latter is mandatory for the construction of organic photovoltaic cells, Ohta et al. highlighted the copper phthalocyanine-fullerene-dyad **1** (Figure 1) to align perfectly homeotropically in a helical columnar liquid crystal with rather low melting temperature[2i,j] and Imahori et al. demonstrated the high charge carrier mobility of compound **2** in a seminal paper,[2c] we decided to resynthesize this class of compounds and study their structure, for which the helicity was proposed based on a so-called H-signal.

Here we uncover the origin of this reflection, which is achieved by X-ray scattering (XRS) on aligned fibers obtained

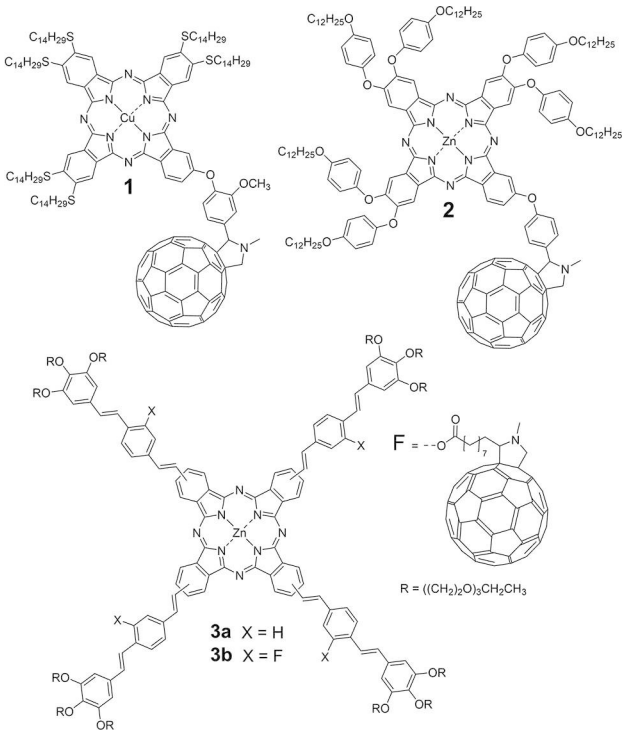

Figure 1. Target molecules **1** (Ohta)[2i,j] and **2** (Imahori)[2c] compared with star mesogens forming a helical columnar phase for the 1:1 mixture of **3a** + **3b**.[7]

[a] *Prof. Dr. M. Lehmann, M. Dechant, D. Weh, E. Freytag*
Institute of Organic Chemistry
University of Würzburg
Am Hubland, 97074 Würzburg (Germany)
E-mail: matthias.lehmann@uni-wuerzburg.de
[b] *Prof. Dr. M. Lehmann*
Center for Nanosystems Chemistry
and Bavarian Polymer Institute
Theodor-Boveri-Weg 4, 97074 Würzburg (Germany)

Supporting information for this article is available on the WWW under https://doi.org/10.1002/cplu.202000540

by extrusion, density measurements, modelling, and electron density reconstruction. The results highlight that instead of a helical structure a lamellar columnar phase is formed, in which the fullerenes segregate in layers and the metal phthalocyanines in columns. Presumably, this is the reason for the balanced hole (1D transport) and electron mobility (2D transport).

The synthesis was performed analogous to the method of the references.[2c,i] The yield of compound **1** could be increased in the last step by 34% using a higher dilution to dissolve a larger portion of the fullerene to guarantee an excess of this starting material. It should be noted, that the isolation of compound **2** is extremely challenging. The mono aldehyde precursor (see Supporting Information) had to be purified with care, since we were not able to separate the side products after the final Prato reaction. The purity and identity is demonstrated by MALDI (HRMS) mass spectrometry, GPC and FT-IR spectroscopy (Figures S1–7). The thermotropic properties were first evaluated by polarized optical microscopy (POM). While compound **1** according to Ohta should clear already at 178 °C, we identified a clearing temperature of 250 °C, which is by 72 °C higher than the reported value. Indeed, the material becomes more fluid at about 178 °C and the thin film does absorb so strongly that birefringence is hardly visible, pretending an isotropic liquid. Ohta et al. highlighted themselves a temperature-dependent XRS study showing defined small angle reflections at 250 °C, which are clearly demonstrating the non-isotropic nature at that temperature.[2j] Therefore, we assume that the material of the present study is identical with the original material investigated by Ohta et al. The alignment of LC films of regular thickness has been studied for which Ohta's observations could be reproduced – dark films could be scratched to exhibit birefringence at the borders of the scratching line (Figure 2A,B). However, we suspected that the dark films originate from the strong absorption of the compound and not from the homeotropic alignment, since no conoscopic picture could be obtained in POM. This proposal has been checked with much thinner films (Figure 2C,D) and indeed dark, but clearly birefringent textures could be discerned at all temperatures, although thinner films should favor homeotropic alignment between two substrates.[3a] Shearing the sample afforded uniformly oriented films, with the highest refractive index oriented perpendicular to the shearing direction (Figure 2E,F). Compound **2** has been described to form a columnar LC phase and freeze to a LC glass; it did not clear but decompose above 200 °C. This behavior has been confirmed for the new samples. Consequently, the POM study reproduced the thermotropic properties of compounds **1** and **2** except for the homeotropic alignment.

In order to get a profound knowledge of the LC structure the materials were studied comprehensively by X-ray scattering techniques. Figure 3 highlights the results for extruded fibers of compounds **1** and **2**. The alignment is discernible by the distinct equatorial and meridional reflections and is especially pronounced for compound **1**. At the equator, five reflections reveal at all temperatures for both compounds and can be attributed clearly to a rectangular phase, for which the 01 reflection is systematically erased (see Table S1). This is in agreement with a planar group of p2gm symmetry.[8] The intensity at the smallest scattering angle was previously described as the H-signal, claimed to correlate with different directions along the samples (see the Supporting Information).[2c,j] In our study, this H-signal in the extruded fibers could be only observed as part of the equator (Figures A,B,C,F). In order to confirm this result, we also

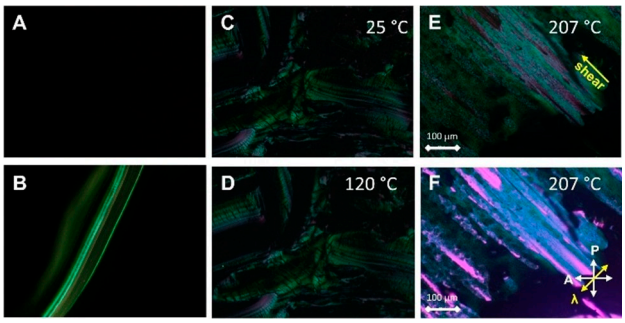

Figure 2. Textures of compound **1**. A) Thick film at 120 °C. B) The same film with a scratch. C, D: thin film cooled from the isotropic phase to 120 °C (C) and 25 °C (D). Thin film at 207 °C sheared along the indicated direction (E) and the texture with an inserted λ-compensation plate (P = polarizer, A = analyzer). The blue birefringence indicate that the highest polarizability is aligned with the compensator plate.

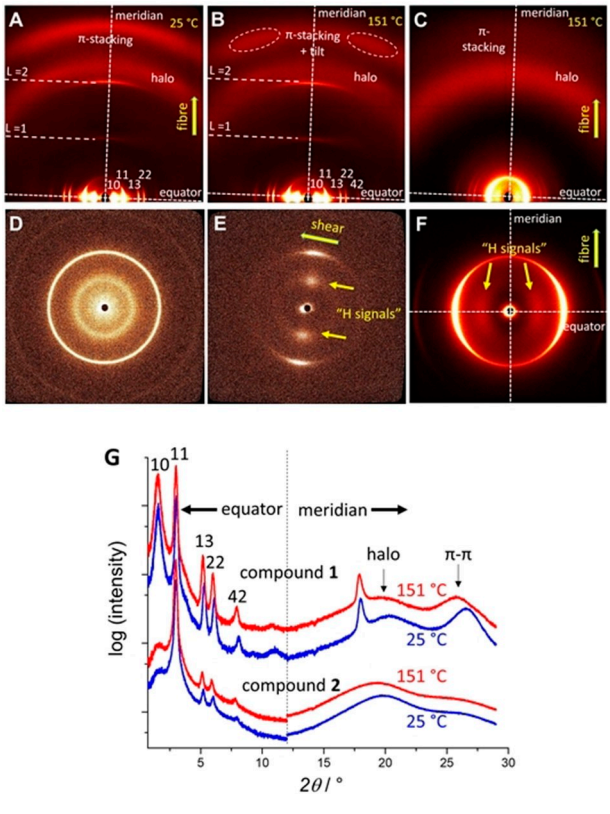

Figure 3. XRS pattern of compounds **1** and **2**. A, B) WAXS pattern of compound **1** at 25 °C and 150 °C. C) WAXS pattern of an extruded fiber of compound **2** at 150 °C. D and E) XRS pattern (SAXS) of a film slowly cooled to ambient temperature (D) and the same sample sheared (E). F) SAXS pattern of compound **2** clearly showing the H-signals at the equator. G: Comparison between the WAXS patterns of compound **1** and **2** at selected temperatures integrated along the equator and the meridian.

prepared a sample by cooling slowly compound **1** from the isotropic phase between two glass substrates to the LC phase in order to obtain possibly a homeotropic aligned material, similar to the previous work of Ohta et al..

Figure 3D shows the diffraction pattern with the X-ray beam orthogonal to the thin film. Compared to the fiber thickness of 0.7 mm, the film is rather thin and the scattering intensity low, and thus, only the strongest reflections at small angles could be observed. They appeared as rings demonstrating the powder-like orientation of the sample, similar to what we observe in the POM study. A sheared sample clearly showed that these three X-ray reflections are positioned at one line (Figure 3E), thus, confirming that the H-signal is indeed an equatorial reflection describing the 2D periodical structure of the LC phase. It is discernible that the 10 reflections possess a larger half-width compared with the 11 reflections (Table S2). SAXS studies on compounds **1** and **2** (Figures S9 and 3F) clearly show that the reflections 10 and 11 are well separated and that the 10 reflections are not superpositions of other reflections, thus, the broader signals are attributed to lower correlation lengths along the *a*-axes of the liquid crystal unit cells.

While the remaining part of the diffraction pattern of compound **2** exhibits only the halo reminiscent of the liquid-like chains and a rather broad signal for the π-π-distances of the phthalocyanine cores, the pattern of compound **1** reveals two extra reflections at the meridian corresponding to distances of 9.9 Å and 4.9 Å. A closer inspection even unravels that there is some very diffuse intensity along layer lines L (L = 1 and 2), indicating 3D periodicity of low correlation length. The distance can be attributed to fullerenes with a van der Waals diameter of 10.6 Å, which are stacked in an interdigitated manner realizing this slightly reduced distance of the fullerene centers. This points to an almost complete nanosegregation of the fullerenes in the structure. In order to obtain further details, we performed electron density reconstructions for the LC phases at 25 °C, which are shown in Figure 4.[9] Both patterns (Figure 4, right) display certain smaller areas of highest electron density (red) connected via a band of high electron density (red (compound **1**) or green/yellow (compound **2**)). Considering the molecular structure of the mesogens, it is clear that the highest electron density is realized by the core with the metal center, while the second highest electron density holds the fullerene areas.Thus, the latter are located at the layers indicated by the red arrows and the phthalocyanines are positioned at the red spots (Figure 4). This clearly uncovers a lamellar columnar phase, in which the fullerenes are packed in layers flanked by the metal phthalocyanine columns. Density measurements are in agreement with five molecules in the unit cell consisting of two columns (see the Supporting Information). The model set-up with the program suite Materials Studio was prepared with ten molecules in the unit cell of the double height (2**c*), thus, with five molecules per column and geometry optimization delivered a nanosegregated structure with high negative non-bonding interaction energy (van der Waals and electrostatic) (see Figure 4 and the Supporting Information) demonstrating the stable nature of this self-assembly. This lamellar columnar phase fits perfectly the 2D structure. Compared with compound **1**, material **2** reveals a lower electron density within the fullerene layers. This can be rationalized with a less well-defined structure. The model shows that the aliphatic chains penetrate the free space within the fullerene layers thus reducing the density (Figure 4B). Residual free space may be also filled at the border of the columns between the phenoxy groups. As a consequence, the material prevents a more pronounced order of the phthalocyanine cores and the fullerenes, which explains the very broad wide angle signals and the absence of the signals attributed to the fullerene stacking.

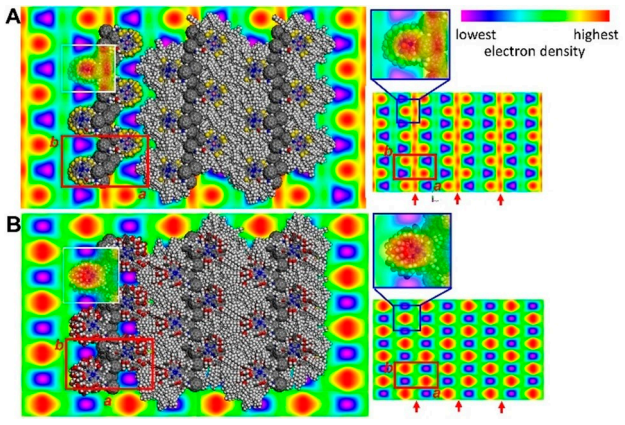

Figure 4. Electron density reconstruction of the p2gm phase of compound **1** (A) and compound **2** (B) at 25 °C. The insets are superpositions of the transparent electron density maps with the model, showing that the highest electron density is located close to the metal center. Enlarged Figure S8 (see the Supporting Information). Red arrows indicate the fullerene layers.

Eventually, Figure 5 details the temperature-dependent behavior of the sample **1**. Figures 5A and B highlight the integration along the equator and the meridian of the XRS patterns. The most pronounced changes are discerned for the π-π distances, which clearly increase with increasing temperature (Figure 5D). The strong changes in the intensity of these reflections are only partially based on the higher disorder at higher temperatures but are correlated with the tilt of the discs along the columns, which shifts the signal continuously out of the fixed integration range, thus, decreasing the signals intensities. The tilt, indicated by the splitted signals already highlighted in Figure 3B, is visualized by the χ-scan (Figure 5F). The fits of these superimposed intensities deliver tilt angles between 8° at ambient temperatures and 24° at 215 °C (Figure 5G). It is a simple consequence of the separating discs with increasing temperature, which can optimize their interaction by the tilt of the aromatic core. The halo is the second signal with a significant change at ambient temperature, at which the chains obviously pack more densely, correlated with the very high viscosity at 25 °C. All other signals shift only slightly, however, systematically with increasing temperature (Figures 5C,D). Parameters *a*, *b* and *c* increase with increasing temperature and consequently, the unit cell volume increases up to a maximum at 185 °C (Figure 5E). While the tilt, the π stacking distance and the *c*-parameter increase continuously, the *a* and *b* parameters decrease above 180 °C, which decreases slightly the cell volume again and point to a lower number *Z* of

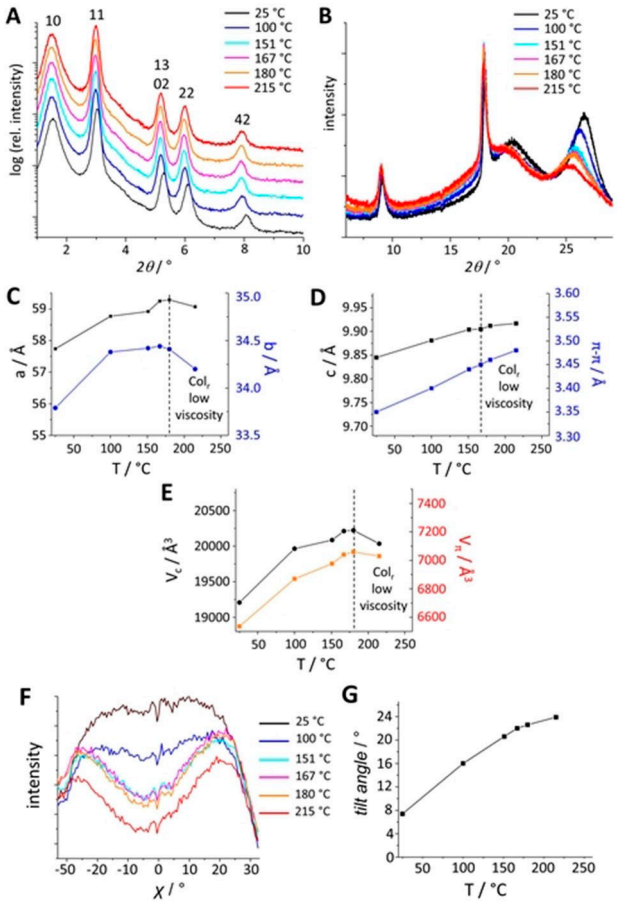

Figure 5. A,B) Temperature-dependent WAXS patterns. A) Integration along the equator. B) Integration along the meridian. C) Cell parameter *a,b* as a function of the temperature. D) Temperature-dependent unit cell parameter *c* and the π-π distance. E) Cell volume and volume corresponding to the π–π distance. F) χ-scan of the π stacking area. The discotic mesogens are slightly tilted at 25 °C and the tilt increases with increasing temperature. This is the reason why the π-signal increases at a fixed integration angle χ in chart (B). G) tilt angle (χ/2) determined from chart (F).

molecules in the unit cells (see Table S1). This rationalizes the lower viscosity and higher fluid nature of the phase at elevated temperatures, although the over-all structure does not considerably change.

Consequently, our comprehensive XRS study rationalizes not only the optical observation: (i) high viscosity at 25 °C; (ii) low viscosity above 180 °C; (iii) planar alignment of the sample but highlights the strong tendency of the fullerenes for an optimized nanosegregation. In contrast to the previously published star-shaped fulleropyrrolidine mesogens and especially to the mixture of star-mesogens **3a** and **3b** (see Figure 1),[6,7] in which the fullerenes are located between the conjugated arms limiting the nanosegregation along the column and at certain positions between the columns, the fullerenes in the dyads **1** and **2** are exposed to the exterior. This allows for a much more efficient nanosegregation of these shape-amphiphiles, because the number of possible interactions between fullerenes is much larger and layer-like packing is feasible. Strong nanosegregation of fullerenes in similar dyads with porphyrin derivatives in a crystalline phase[4] and lamellar fullerene self-assemblies are reported,[10,11] but the present lamellar columnar phase is unique. With this model in mind, it can be understood why the additional phenyloxy groups of Imahori's mesogen **2** inhibit a higher order in the LC phase. It is important to note, that although the phenoxy groups extend the mesogen size, the unit cell parameters are almost identical for both compounds **1** and **2**. These groups prevent an efficient π-π stacking of the phthalocyanines and impact strongly on the order of fullerene packing. The model (Figure 4B) clearly indicates that for compound **2** the aliphatic chains enter to the free volumes between the fullerenes much stronger than for compound **1** leading to the loss of the regular packing and the signals along the meridian. Therefore, it is highly interesting that this rather disordered material possess high ambipolar and balanced charge carrier mobilities in the annealed film, demonstrated by the time of flight method.[2c] The present model may explain naturally the high balanced charge carrier mobility of electrons since here the percolation pathways are two-dimensional and charge trapping can be more easily circumvented. The mobility of the holes is usually high along the 1D columns.[1]

Eventually, we would like to emphasize that Ohta's compound **1** has a much better defined LC structure–well defined π-stacking and fullerene packing–and the synthesis and isolation is much easier compared with Imahori's compound **2**. Compound **1** may therefore be proposed to be excellent for either photo sensitive devices in a transistor set-up, thus, with planar aligned material, or photovoltaic devices for homeotropically aligned LC phases. It provides also the possibility to improve the electric properties by blending fullerene derivatives, in order to increase the fullerene layer thickness and decrease the recombination probability. To the best of our knowledge, no such applications have been reported to date. Beside the synthetic challenge of producing non-symmetric phthalocyanine derivatives, the homeotropic alignment is an important issue, which we could not achieve with conventional methods.

In contrast to the reported helical models for phthalocyanine-fullerene dyads, we confirmed for two samples a lamellar columnar phase, in which the fullerenes nanosegregate into layers flanked by phthalocyanine columns. This 2D structure is proposed to be responsible for the high ambipolar and balanced charge carrier mobilities found by Imahori and Shimizu et al.. These structures are extremely promising for photovoltaic or photo sensor applications if their alignment can be controlled. This is work, which is currently in progress.

Acknowledgements

We are grateful to the Deutsche Forschungsgemeinschaft (DFG) for their financial support within the LE1571/8-1. Open access funding enabled and organized by Projekt DEAL

Conflict of Interest

The authors declare no conflict of interest.

Keywords: Donor–acceptor dyads · fullerenes · liquid crystals · nanosegregation · shape-amphiphiles

[1] a) S. Sergeyev, W. Pisula, Y. H. Geerts, *Chem. Soc. Rev.* **2007**, *36*, 1902–1929; b) T. Wöhrle, I. Wurzbach, J. Kirres, A. Kostidou, N. Kapernaum, J. Litterscheidt, J. C. Haenle, P. Staffeld, A. Baro, F. Giesselmann, S. Laschat, *Chem. Rev.* **2016**, *116*, 1139–1241; c) J. W. G. Goodby, P. J. Collings, J. Wiley, Sons, T. Kato, C. Tschierske, H. F. Gleeson, E. P. Raynes, *Handbook of Liquid Crystals, Vol. 8*, 2nd ed., Wiley-VCH, Weinheim, **2014**.

[2] a) Y. H. Geerts, O. Debever, C. Amato, S. Sergeyev, *Beilstein J. Org. Chem.* **2009**, *5*, 49; b) M. Ince, M. V. Martínez-Díaz, J. Barberá, T. Torres, *J. Mater. Chem.* **2011**, *21*, 1531–1536; c) H. Hayashi, W. Nihashi, T. Umeyama, Y. Matano, S. Seki, Y. Shimizu, H. Imahori, *J. Am. Chem. Soc.* **2011**, *133*, 10736–10739; d) T. Kamei, T. Kato, E. Itoh, K. Ohta, *J. Porphyrins Phthalocyanines* **2012**, *16*, 1261–1275; e) M. Shimizu, L. Tauchi, T. Nakagaki, A. Ishikawa, E. Itoh, K. Ohta, *J. Porphyrins Phthalocyanines* **2013**, *17*, 264–282; f) L. Tauchi, T. Nakagaki, M. Shimizu, E. Itoh, M. Yasutake, K. Ohta, *J. Porphyrins Phthalocyanines* **2013**, *17*, 1080–1093; g) A. Ishikawa, K. Ono, K. Ohta, M. Yasutake, M. Ichikawa, E. Itoh, *J. Porphyrins Phthalocyanines* **2014**, *18*, 366–379; h) M. Yoshioka, K. Ohta, Y. Miwa, S. Kutsumizu, M. Yasutake, *J. Porphyrins Phthalocyanines* **2014**, *18*, 856–868; i) A. Watarai, S. n. Yajima, A. Ishikawa, K. Ono, M. Yasutake, K. Ohta, *ECS Trans.* **2015**, *66*, 21–43; j) A. Watarai, K. Ohta, M. Yasutake, *J. Porphyrins Phthalocyanines* **2016**, *20*, 1444–1456.

[3] a) T. Brunet, O. Thiebaut, E. Charlet, H. Bock, J. Kelber, E. Grelet, *EPL* **2011**, *93*, 16004; b) J. Eccher, W. Zajaczkowski, G. r. C. Faria, H. Bock, H. Von Seggern, W. Pisula, I. H. Bechtold, *ACS Appl. Mater. Interfaces* **2015**, *7*, 16374–16381; c) J. Eccher, G. C. Faria, H. Bock, H. von Seggern, I. H. Bechtold, *ACS Appl. Mater. Interfaces* **2013**, *5*, 11935–11943.

[4] a) C. L. Wang, W. B. Zhang, H. J. Sun, R. M. Van Horn, R. R. Kulkarni, C. C. Tsai, C. S. Hsu, B. Lotz, X. Gong, S. Z. Cheng, *Adv. Energy Mater.* **2012**, *2*, 1375–1382; b) C. L. Wang, W. B. Zhang, R. M. Van Horn, Y. Tu, X. Gong, S. Z. Cheng, Y. Sun, M. Tong, J. Seo, B. B. Hsu, *Adv. Mater.* **2011**, *23*, 2951–2956.

[5] M. Loi, P. Denk, H. Hoppe, H. Neugebauer, D. Meissner, C. Winder, C. Brabec, N. S. Sariciftci, A. Gouloumis, P. Vázquez, T. Torres, *Synth. Met.* **2003**, *137*.

[6] a) M. Lehmann, M. Hügel, *Angew. Chem. Int. Ed.* **2015**, *54*, 4110–4114; *Angew. Chem.* **2015**, *127*, 4183–4187; b) M. Hügel, M. Dechant, N. Scheuring, T. Ghosh, M. Lehmann, *Chem. Eur. J.* **2019**, *25*, 3352–3361.

[7] M. Lehmann, M. Dechant, M. Holzapfel, A. Schmiedel, C. Lambert, *Angew. Chem. Int. Ed.* **2019**, *58*, 3610–3615.

[8] M. I. Aroyo, *International Tables of Crystallography, Vol. 6*, 6th ed., Wiley Chichester **2006**.

[9] C. Tschierske, *Electron density reconstruction software "Electron Density Map"* Halle University, Germany.

[10] X. Zhang, C. H. Hsu, X. Ren, Y. Gu, B. Song, H. J. Sun, S. Yang, E. Chen, Y. Tu, X. Li, *Angew. Chem. Int. Ed.* **2015**, *54*, 114–117; *Angew. Chem.* **2015**, *127*, 116–119.

[11] D. Felder Flech, D. Guillon, B. Donnio, *Fullerene-containing Liquid Crystals in Handbook of Liquid Crystals*, Vol. 5, 2nd ed. (Eds.: J. W. Goodby, P. J. Collings, T. Kato, C. Tschierske, H. Gleeson, P. Raynes), Wiley-VCH, Weinheim, **2014**, Chapter 6, pp. 317–361.

Manuscript received: July 21, 2020
Revised manuscript received: August 1, 2020
Accepted manuscript online: August 3, 2020